Front. Earth Sci. 2023, 17(2): 455–469
https://doi.org/10.1007/s11707-022-0998-x

RESEARCH ARTICLE

Quartz types, genesis and their geological significance within the Wufeng-Longmaxi Formation in north-western Hunan, China

Ke ZHANG[1,2,3], Shuheng TANG (✉)[1,2,3], Zhaodong XI[1,2,3], Yapei YE[1,2,3]

1 School of Energy Resource, China University of Geosciences (Beijing), Beijing 100083, China
2 Key Laboratory of Marine Reservoir Evolution and Hydrocarbon Enrichment Mechanism, Ministry of Education, Beijing 100083, China
3 Key Laboratory of Strategy Evaluation for Shale Gas, Ministry of Land and Resources, Beijing 100083, China

Abstract Quartz is an important mineral component in the Late Ordovician – Early Silurian Wufeng-Longmaxi Formation with various forms and sources and has a significant impact on the properties of shale gas reservoirs. In this study, geochemical analysis, scanning electron microscopy (SEM) observation, and rock mechanics testing were performed on shale samples from the Wufeng-Longmaxi Formation in north-western Hunan, South China. Quartz is classified into four types based on morphological features and cathodoluminescence (CL) images under SEM – terrigenous detrital quartz, quartz overgrowths, biogenic skeletal quartz and microquartz. The quartz in Upper Longmaxi Formation is predominantly of terrigenous origin and contains a small amount of quartz formed by clay transformation. The quartz in the Wufeng-Lower Longmaxi Formation is predominantly biogenic. The biogenic quartz has a direct effect on organic matter (OM) abundance, pore structure and brittleness. It is indicated by the positive correlation with TOC content and biogenic Ba content that biogenic quartz-rich strata have high paleoproductivity. The rigid frameworks formed by biogenic quartz during the early diagenesis stage facilitated the preservation of the primary pores. The interparticle pores of biogenic quartz are the space for OM preservation and migration, creating conditions for the development of OM pores. Additionally, the calculated brittleness index (BI) shows a positive correlation with biogenic quartz content, indicating that layers rich in biogenic quartz are more conducive to fracture. Therefore, the Wufeng-Lower Longmaxi Formation has higher OM content, porosity and represents a more favorable exploration and development target.

Received February 13, 2022; accepted June 12, 2022

E-mail: tangsh@cugb.edu.cn

Keywords quartz, silica source, porosity, organic matter, rock mechanics

1 Introduction

The marine shales of the Late Ordovician Wufeng Formation–Early Silurian Longmaxi Formation from the upper Yangtze Platform are widely distributed and represent the main exploration target of shale gas in the Sichuan Basin. Significant progress has been made in the exploration and development of the Wufeng-Longmaxi Formation during the last years (Shan et al., 2017; Zou et al., 2020). Being one of the most common minerals in shales, quartz has an important influence on the quality of shale reservoirs. Over the last few years, many scholars have conducted detailed studies on quartz and have obtained some conclusions regarding the silica origin of quartz and the influence of quartz on reservoirs (Peltonen et al., 2009; Xi et al., 2022). Recent studies have shown that microquartz in the Late Cretaceous mudstones from the North Sea is derived from silica released by clay transformation (Peltonen et al., 2009; Thyberg et al., 2010). Schieber et al. (2000) analyzed the Late Devonian shales from the eastern United States and concluded that most of the quartz in shales formed during diagenesis, the source of silica is associated with the dissolution and reprecipitation of siliceous biogenic skeletons. Additionally, silica can also be derived from the alteration of K-feldspar and plagioclase (Lynch, 1997; Metwally and Chesnokov, 2012). Milliken and Olson (2017) classified the multiple forms of quartz in the Mowry Shale as extrabasinal detrital silt, replacement of skeletal debris, minor overgrowth on detrital quartz and replaced radiolaria, pore-filling in the intragranular pores of allochems and authigenic microquartz that is dispersed

through the clay-sized matrix; Niu et al. (2018) analyzed the Niutitang shale and identified four different types of quartz as angular to sub-rounded silt-size quartz grains, quartz filled in sponge spicules, quartz overgrowths and microcrystalline quartz. The depositional environment and tectonic setting of the shales in the study area are not completely consistent with previous studies. There are differences in the type and content of quartz in different shales. Thus, it is necessary to clarify the quartz categories and formation mechanisms in the study area, which is important to reconstruct the sedimentary history of the shale sequence. The most commonly used methods to accurately analyze the quartz types and understand the silica origin are SEM and CL images (Barghoorn and Tyler, 1965; Milliken et al., 2016), main, trace and rare earth element (REE) concentrations, (Shimizu and Masuda, 1977; van den Boorn et al., 2007) and δ^{30}Si data (Reynolds and Verhoogen, 1953; Tatzel et al., 2017).

The influence of quartz on reservoir properties is manifested in different ways, including its porosity, permeability, pore structure and brittleness (Milliken et al., 2016). Quartz from clay mineral transformation reduces reservoir porosity and increases the anisotropy of the mudstone during burial (Thyberg et al., 2010). OM pores have predominantly nanoscale dimensions and have been recognized as an important component of shale pore systems. The main substrate for OM pores development is represented by migrated OM in authigenic quartz aggregates (Curtis et al., 2012; Pommer and Milliken, 2015; Zhao et al., 2017). Biogenic quartz is transformed from opal A to opal CT during its formation, eventually forming quartz cements. This process has an effect on the mechanical properties of the rock and directly influences the brittleness and fracturability of the formation (Ishii et al., 2011; Milliken et al., 2012). The shales of the Wufeng-Longmaxi Formation from the Sichuan Basin are rich in quartz minerals which have the characteristics of high-quality reservoirs. Understanding the relationship between quartz and OM content, pore development, and rock mechanics properties is of great importance for sedimentary environment analysis and favorable reservoir prediction.

The objective of this paper is to classify the quartz from the Wufeng-Longmaxi Formation shales and to identify the silica origin. The effect of quartz on pore space and OM enrichment in shale reservoirs is also explored in order to provide new ideas for the prediction of favorable source rocks.

2 Geological setting

During the Late Ordovician–Early Silurian, the western part of the Yangtze Platform suffered tectonic compression as a result of the Caledonian orogeny, leading to the formation of the Xuefeng Uplift, the Chuanzhong Uplift and the Qianzhong Uplift (Fig. 1). The open ocean environment had gradually transitioned into a confined ocean environment surrounded by uplift, accompanied by a relative rise in sea level (Zhou et al., 2015). The

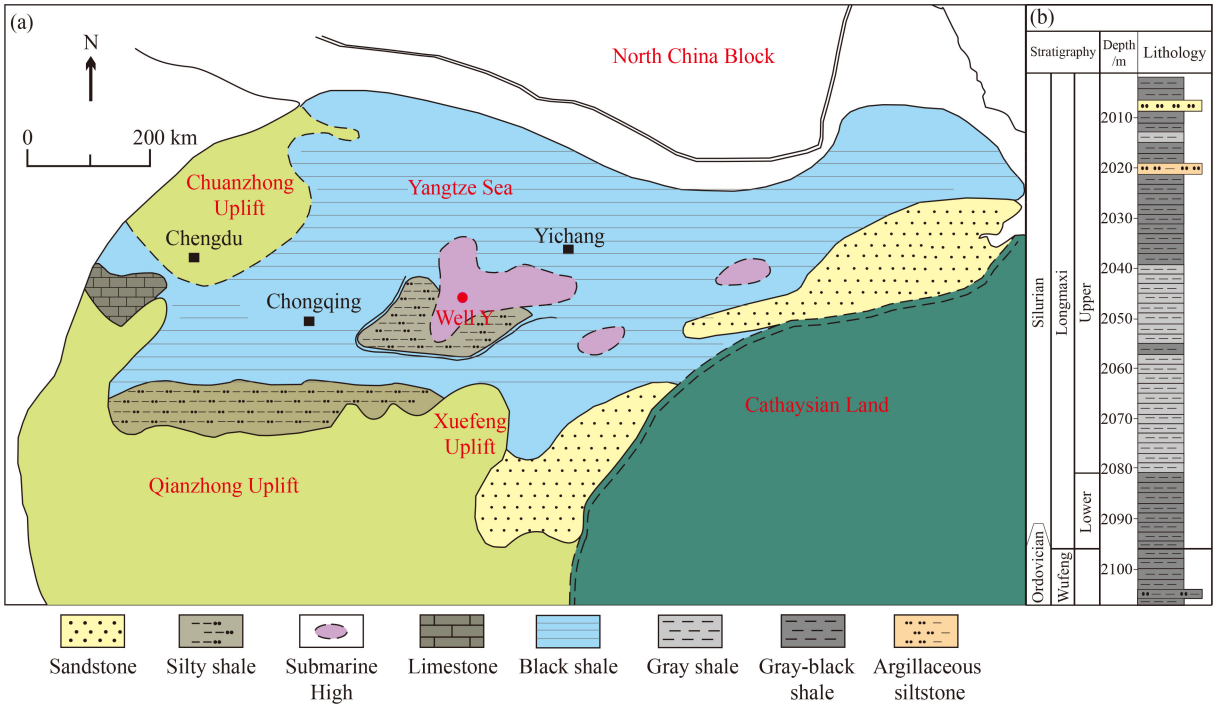

Fig. 1 (a) Paleogeographic map of the Yangtze area during Early Silurian time highlighting the lithofacies distribution and the position of well Y. (b) Lithostratigraphic column of the Wufeng-Longmaxi Formation in well Y (modified from Xu et al., 2004).

deposition of sediments in the south-eastern Sichuan Basin had taken place in a predominantly anoxic and low-energy depositional environment. Black shales were widely distributed, although their thickness decreases significantly due to large scale sea erosion in the south-western part of the basin. The organic-rich shales of the Wufeng-Longmaxi Formation are the most important layers for economic and commercial purposes (Liu et al., 2012). The depositional environment of Wufeng Formation in the study area is deep shelf environment (Xu et al., 2004). The lithology is mainly siliceous shale, with a thickness of only a several meters. Subsequent sea retreats had caused sedimentary waters to become shallow. The sedimentary environment of Upper Longmaxi Formation shifted to shallow shelf and the sediment source mainly originated from the Xuefeng Uplift in the south-east. The lithology is dominated by gray shale, locally interspersed with siltstone. The thickness distribution ranges from 50 to 500 m (Zhao et al., 2017).

3 Sample and methods

Shale samples were taken from the Wufeng-Longmaxi Formation in well Y. X-ray Diffraction (XRD) analyses, major, minor and trace element analyses, TOC content tests, SEM observations, porosity determination, and triaxial compression tests were performed.

XRD analyses were performed using a Rigaku SmartLab9 X-ray diffractometer. The sample powder size was less than 40 μm and the test conditions were CuKα radiation, 40 kV operating voltage, 0.02° scan step, and 2°/min scan speed. The samples were scanned in the range of 5°–45°. The contents of clay and non-clay minerals were derived separately using the K-value method (matrix-flushing method) and the adiabatic principle (Chung, 1974).

Major and minor element concentrations were analyzed using an XRF Spectrometer. The dry sample powder was crushed to a size smaller than 200 mesh, followed by calcination at 1000°C for 4 h. Afterwards, 0.5 g of the sample was mixed with 4 g of anhydrous lithium tetraborate, 0.4 g of lithium fluoride and 0.3 g of amine nitrite in a platinum crucible and treated with a lithium bromide solution. After that, the sample was dried on an electric heating plate. The crucible was melted at 1150°C and finally measured using X-ray fluorescence spectrometry with an accuracy of less than 3%. Rare earth elements (REEs) and other trace elements were measured using inductively coupled ion mass spectrometry (ICP-MS) (Li et al., 2019).

The identification of the main mineral phases and the pore structure was done using a Zeiss Merlin field emission scanning electron microscope. The samples were prepared by applying the argon ion polishing technique according to the SY/T5162-2014 standard. The samples were pre-sanded with coarse to fine-grained sandpaper and placed into the ion thinning apparatus to bombard the surface of the sample with the argon ion beam. Afterwards, the sample was mounted on the sample table with conductive adhesive and sprayed with gold treatment for examination. The accelerating voltage was 10 Kv, and the detector was a backscattered electron.

The TOC content was determined by Leco CS230 carbon/sulfur analyzer. The samples were ground to a particle size of less than 0.2 mm, weighed, and then 1 mol/L hydrochloric acid was added to remove carbonates. Then wash the sample to neutral with distilled water and put it into 60°C–80°C oven to dry. Finally, the samples were sent to the carbon/sulfur analyzer for testing.

Porosity was obtained by using apparent density in combination with skeletal density according to Chalmers et al. (2012) (Porosity = (skeletal density − apparent density)/skeletal density × 100%). Coated paraffin was used to measure the apparent density of each shale sample weighing around 50 g, and the skeletal density was determined using a helium pycnometer after the paraffin was removed.

The triaxial compression test was conducted based on the GB/T 23561.9-2009 standard. The samples were made into a cylinder of 25 mm in diameter and 50 mm in length. All shale samples were dried at 100°C for 12 h prior to testing. The circumferential pressure was maintained at 40 MPa, while the longitudinal load was applied at a loading rate of 0.5–1.0 MPa/s until the specimen was damaged. The load data were automatically recorded by a computer. The elastic modulus and Poisson's ratio were obtained by measuring the axial and transverse deformation by sensors (Li et al., 2020, 2022).

4 Results

4.1 TOC content, major elements and mineral compositions

The TOC content of Wufeng-Longmaxi Formation ranges from 0.2 wt% to 2.5 wt%, with an average value of 1.3 wt% (Table 1). The TOC > 1.5 wt% section is concentrated in Wufeng-Lower Longmaxi Formation. The concentrations of the major elements Si and Al ranged from 21.20% to 39.46% and 2.13%–10.32%, with an average of 31.82% and 7.70%, respectively. The Si content in Wufeng-Lower Longmaxi Formation is higher than that in Upper Longmaxi Formation, whereas the Al content in Upper Longmaxi Formation is higher than that in Wufeng-Lower Longmaxi Formation (Table 1).

The mineral compositions of the shale in the study area are quartz, clay minerals, feldspar (K-feldspar and plagioclase), calcite, dolomite, and pyrite. Quartz contents range from 25.8% to 86.4%, with an average value of 45.2%; clay minerals contents range from 15.2%

Table 1 Results of various parameters of Wufeng-Longmaxi shale

Samples	Depth/m	TOC/wt%	Al/%	Si/%	Fe/%	Mn/%
Y1	2002.80	0.18	9.33	21.20	4.31	0.03
Y2	2007.13	0.20	9.15	26.15	4.62	0.04
Y3	2015.60	0.21	9.73	27.04	4.64	0.04
Y4	2027.90	0.21	9.73	27.08	4.59	0.04
Y5	2033.75	0.31	9.66	27.14	4.76	0.05
Y6	2047.70	0.72	10.02	27.75	5.08	0.04
Y7	2053.35	0.17	9.80	28.06	4.81	0.04
Y8	2060.40	0.25	9.79	28.11	4.98	0.05
Y9	2064.30	0.34	9.73	28.15	5.49	0.05
Y10	2069.50	0.15	10.04	28.30	4.79	0.04
Y11	2074.10	0.19	9.80	28.31	4.77	0.05
Y12	2083.00	1.29	9.43	28.32	5.12	0.04
Y13	2083.50	1.58	9.22	28.45	5.11	0.04
Y14	2086.90	2.01	8.40	28.75	4.52	0.03
Y15	2089.30	2.25	6.74	28.84	4.26	0.04
Y16	2090.10	2.01	6.56	28.92	3.50	0.03
Y17	2091.30	1.37	10.32	28.98	3.81	0.02
Y18	2092.10	1.88	6.20	29.32	3.07	0.03
Y19	2093.00	1.58	6.96	29.46	3.03	0.03
Y20	2093.60	1.81	8.09	29.50	3.59	0.02
Y21	2094.60	1.73	6.90	29.53	3.21	0.03
Y22	2095.80	1.72	7.02	29.96	3.10	0.03
Y23	2096.60	5.13	4.85	30.34	3.84	0.19
Y24	2097.00	1.19	7.28	30.65	3.04	0.02
Y25	2097.80	1.44	6.45	31.05	3.53	0.02
Y26	2098.33	1.42	6.28	31.31	3.69	0.02
Y27	2099.20	1.44	7.37	31.37	4.61	0.03
Y28	2099.70	1.43	7.60	31.38	3.23	0.04
Y29	2100.00	1.93	8.17	32.09	3.05	0.04
Y30	2101.40	1.81	3.59	32.23	1.64	0.03
Y31	2101.80	1.43	8.00	32.45	3.54	0.02
Y32	2102.80	2.34	4.32	35.32	1.94	0.02
Y33	2102.00	1.90	2.13	35.48	1.13	0.03
Y34	2101.80	2.44	6.53	35.90	2.93	0.02
Y35	2104.00	0.78	4.48	36.81	2.58	0.03
Y36	2105.50	1.05	5.61	37.73	2.78	0.02
Y37	2106.20	1.01	4.07	39.46	2.68	0.05

to 53.2%; the contents of the remaining minerals are much lower than those of quartz and clay minerals, usually less than 10%.

4.2 Quartz type

Based on high-resolution SEM images, quartz can be classified into the following 4 categories according to its morphology and genesis: 1) terrigenous detrital quartz; 2) quartz overgrowths; 3) biogenic skeletal quartz; 4) microquartz, which can be divided into two subclasses: clay matrix-dispersed microquartz and microquartz cements. Detailed descriptions are explained as follows.

4.2.1 Terrigenous detrital quartz

Terrigenous detrital quartz crystals are characterized by angular or sub-angular forms, which indicates short sediment transport distances. Their dimensions vary from a few microns to tens of microns and the crystals are easily distinguished by CL, which displays a strong luminescence in the CL images (Figs. 3(a) and 3(b)). Terrigenous detrital quartz is mainly derived from detrital material outside of the basin. The terrigenous detrital component of the shale is a product of physicochemical weathering of the parent rock mixed with a small amount of volcanic ash and organic material of terrestrial origin, which was transported into the basin mainly by fluvial and eolian action (Wright, 2001).

4.2.2 Quartz overgrowths

Quartz overgrowths are widespread in Upper Longmaxi shale and are present as cement around terrigenous quartz, usually formed on the surface of mineral grains during late diagenesis (Dong et al., 2019). The quartz overgrowths display a weak luminous color in the CL images, while the terrigenous detrital quartz is strongly luminous (Figs. 3(c) and 3(d)). The difference in luminescence intensity between them can be distinguished by the presence of a clear demarcation line on the CL image.

4.2.3 Biogenic skeletal quartz

Biogenic skeletal quartz is transformed from siliceous biological carapaces (radiolarians, sponge spicules, etc.) which can be partially observed as a distinct biological structure under SEM (Milliken et al., 2016). Some of the radiolarians are preserved in their original spherical, ellipsoidal shape (Figs. 4(a) and 4(b)). This is because the biological skeleton was replaced by quartz during the diagenetic stage, preserving the original shape (Xu et al., 2021).

4.2.4 Microquartz

Authigenic microquartz is the second most common type of quartz in the analyzed samples after terrestrial detrital quartz, and is divided into two subclasses based on its morphology, mode of occurrence and genesis.

1) Clay matrix-dispersed microquartz

A large number of micro-sized quartz crystals dispersed in the clay matrix were observed in the samples from Upper Longmaxi Formation (Fig. 4(c)). The size usually

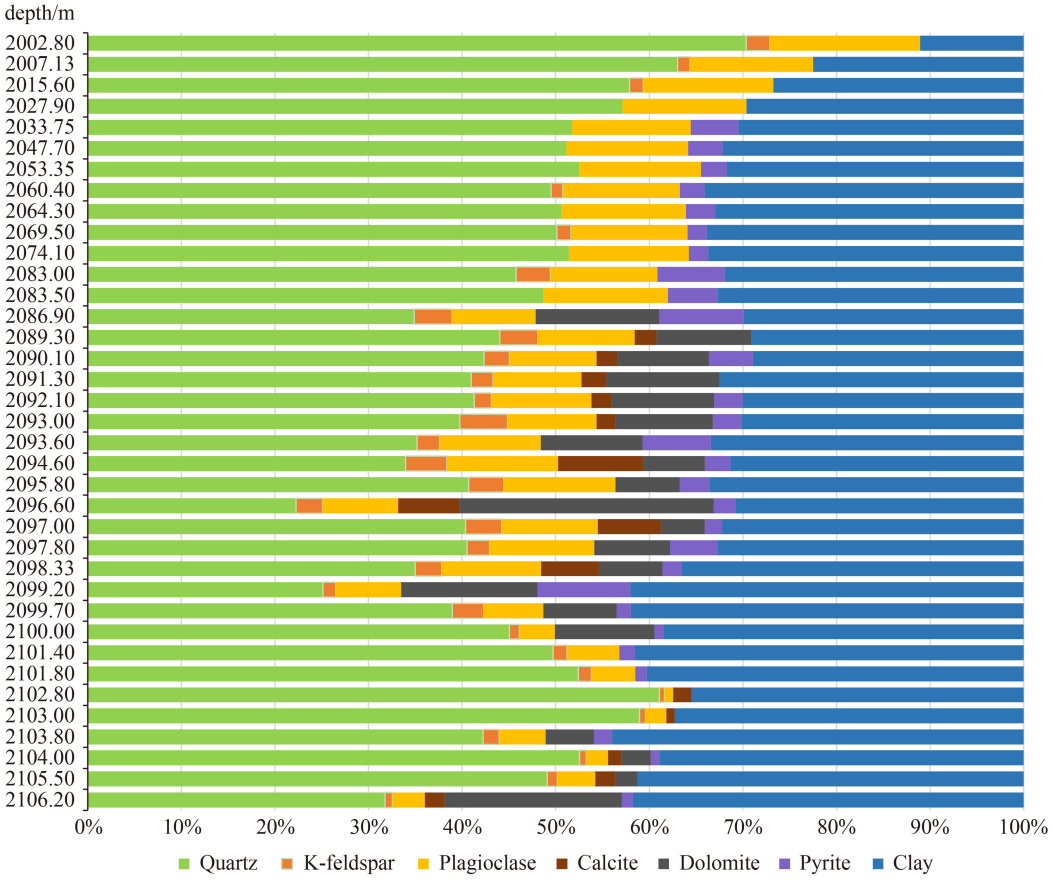

Fig. 2 Mineral composition (wt%) of the shale samples from the Wufeng-Longmaxi Formation based on XRD. Clay minerals and quartz are the main minerals.

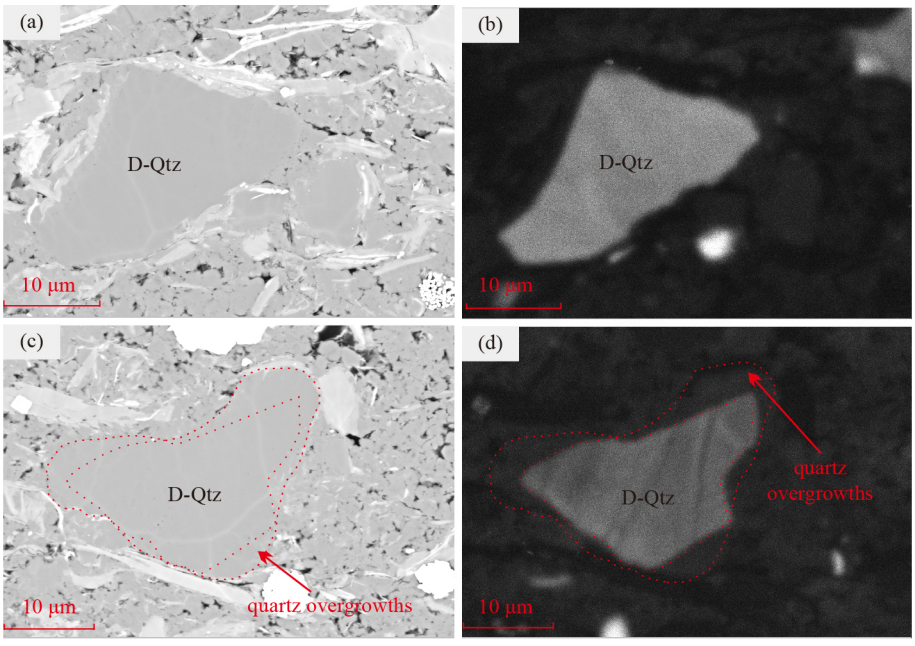

Fig. 3 SEM and CL images of terrigenous detrital quartz (D-Qtz) and quartz overgrowths. (a) Terrigenous detrital quartz is characterized by angular and subangular shapes. (b) Terrigenous detrital quartz is defined by a strong luminous color in the CL image. (c) Terrigenous detrital quartz and quartz overgrowths crystallizing around it. (d) Quartz overgrowths do not display luminescence in the CL image, therefore the boundary between quartz overgrowths and terrigenous detrital quartz is clearly visible.

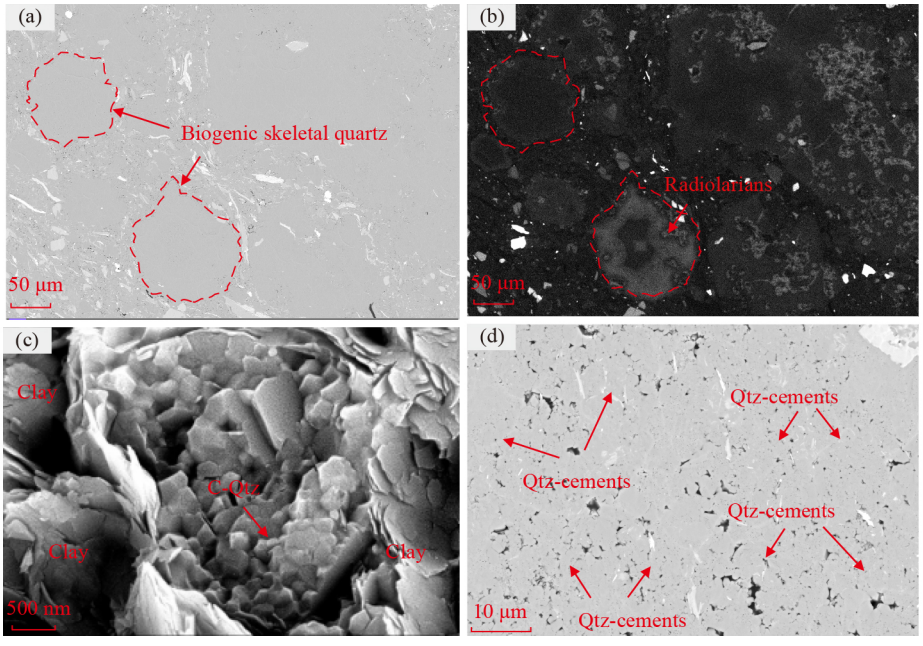

Fig. 4 SEM and CL images of biogenic skeletal quartz and microquartz. (a) Biogenic skeletal quartz. (b) Radiolarian skeleton under SEM-CL showing silica-filled interior. (c) Authigenic microquartz scattered in clay matrix in unpolished samples. (d) Microquartz cements (Qtz-cements).

varies from 1 μm to 3 μm, while the cathodoluminescence is weak. This type of quartz is mainly manifested as discrete spherical grains or aggregated in clusters distributed in the clay matrix, commonly in association with illite (Boles and Franks, 1979; Metwally and Chesnokov, 2012).

2) Microquartz cements

Microquartz cements are poorly crystallized and amorphous in shape, appearing as cements in shale (Williams et al., 1985). Microquartz cements are the most frequent form of microquartz in the Wufeng-Lower Longmaxi Formation and have dimensions that vary in diameter from 1 μm to 4 μm (Fig. 4(d)). The intergranular pores are well developed and filled with a significant amount of OM.

4.3 Pores associated with quartz

In this study, the pores associated with quartz were classified into four distinct categories. 1) Intraparticle pores, which are produced by the erosion of quartz grains when the quartz crystals encounter alkaline solutions during the diagenetic stage. The pores in terrigenous detrital quartz have irregular shapes and are characterized by sizes less than 1 μm (Fig. 5(a)); 2) Interparticle pores, which are pores located between the grains of various quartz crystals. These pores have highly variable sizes, ranging from a few hundred nanometers to several microns, as well as irregular shapes. The larger interparticle pores are usually filled with OM. Interparticle pores are the most common type of pores encountered in microquartz crystals (Figs. 5(b) and 5(c)); 3) Micro-fractures in quartz grains, which were formed by mechanical compaction inducing the quartz to break. The length of the micro-fractures varies from a few microns to several tens of microns (Fig. 5(d)); 4) Shrinkage micro-fractures, which are micro-fractures formed by the shrinkage of OM or clay located at the proximity of quartz grains (Fig. 5(d)).

5 Discussion

5.1 Source of silica for quartz

There are several sources of silica for the described quartz types from the analyzed samples, which can be explored by using geochemical elemental ratios and by analyzing the lithofacies composition of the shales. The relationship between Si and Al can determine quartz contents that are higher than the average contents in a detrital sedimentary environment. Samples plotted near the illite Si/Al line are dominated by terrigenous detrital quartz, while samples situated above the illite Si/Al line are enriched in authigenic quartz (Rowe et al., 2008). All of the analyzed samples from Upper Longmaxi Formation fall near the Si/Al line, while the samples from the Wufeng-Lower Longmaxi Formation have higher Si/Al values, therefore are situated above the Si/Al line (Fig. 6). This leads to the conclusion that Upper Longmaxi Formation shales are dominated by terrigenous detrital quartz. The Wufeng-Lower Longmaxi Formation is characterized by the presence of a significant amount of authigenic quartz that was formed during diagenesis. The possibility to determine detrital silica input was explored by correlating SiO_2 with Zr or Ti (Gambacorta et al., 2016). The Zr contents are related to the heavy mineral zircon, which represents a good indicator of terrigenous input. SiO_2 in Upper Longmaxi Formation is weakly positively correlated with Zr (R^2 = 0.2596) (Fig. 7). This indicates that not all the quartz in Upper Longmaxi Formation is terrigenous detrital quartz, and there is some authigenic quartz. There is little correlation between SiO_2 and Zr in Wufeng-Lower Longmaxi Formation (R^2 = 0.0696). This indicates that shale in Wufeng-Lower Longmaxi Formation contains less terrigenous detrital quartz, mostly

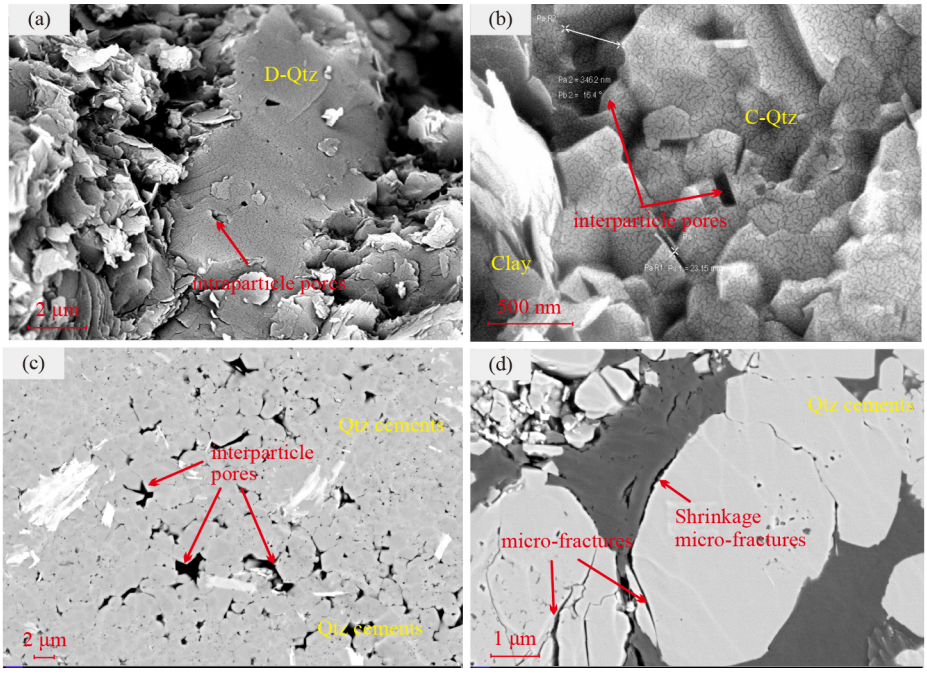

Fig. 5 Different types of pores associated with quartz under SEM. (a) Intraparticle pores formed by the dissolution of terrigenous detrital quartz (D-Qtz) in unpolished samples. (b) Interparticle pores located between clay matrix-dispersed microquartz (C-Qtz) in unpolished samples. (c) Interparticle pores positioned between microquartz cements (Qtz-cements). (d) Micro-fractures in microquartz grains and shrinkage micro-fractures located between microquartz and OM.

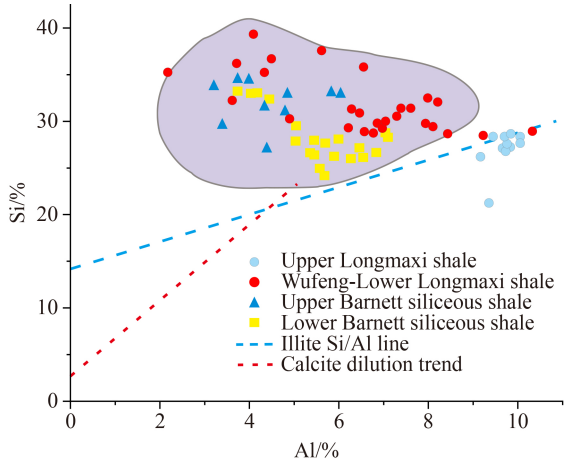

Fig. 6 Si-Al correlation diagram for the Wufeng-Longmaxi Formation shales (modified from Rowe et al., 2008).

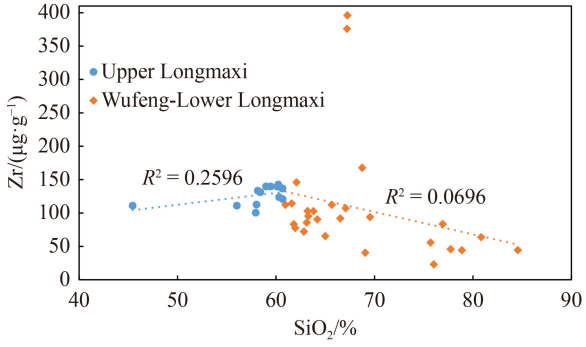

Fig. 7 Correlation diagram between Zr and SiO_2.

authigenic quartz.

The most common sources of silica for the precipitation of authigenic quartz are hydrothermal input, clay mineral transformations and biogenesis. Previous studies have shown that modern submarine hydrothermal silica deposition is directly influenced by two parameters. The interaction of upwelling hot thermal fluids with the cold seawater leads to the precipitation of supersaturated amorphous silica. To better constrain the hydrothermal genesis of quartz, the Al-Fe-Mn ternary diagram was used (Adachi et al., 1986). All of the analyzed samples fall into the non-hydrothermal area (Fig. 8), indicating that none of the quartz from the shales of the Wufeng-Longmaxi Formation is of hydrothermal origin.

The transformation of smectite to illite results in the formation of SiO_2, which can be expressed in the following Eq. (1) (Boles and Franks, 1979):

$$K^+ + \text{Smectite} \rightarrow \text{Illite} + Na^+ + Ca^{+2} + Fe^{+2} + Mg^{+2} + Si^{+4} + OH^- + H_2O. \quad (1)$$

The equation is considered to be a dissolution-precipitation reaction. The smectite particles dissolve in order to produce authigenic illite, while the resulting SiO_2

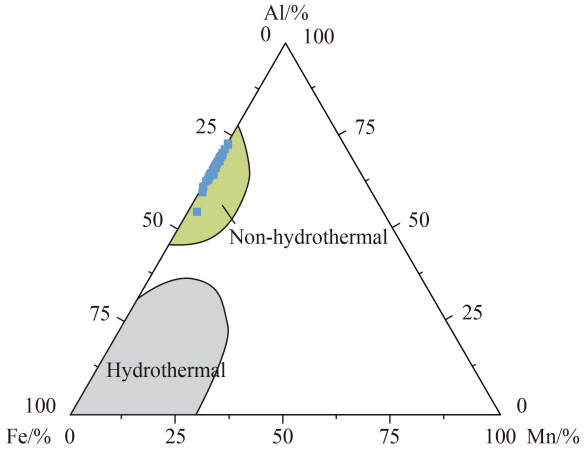

Fig. 8 Al-Fe-Mn ternary diagram of the shale samples from the Wufeng-Longmaxi Formation. The gray area indicates non-hydrothermal genesis, while the green area indicates hydrothermal genesis. All samples fall into the non-hydrothermal area (modified from Adachi et al., 1986; Yamamoto, 1987).

rapidly precipitates in the vicinity of the illite. Some researchers have experimentally simulated the transformation process and obtained two types of quartz with different morphologies. The first type of quartz is granular microquartz within a clay matrix, and the other one is flake quartz covered with granular quartz or other components (Metwally and Chesnokov, 2012). This indicates that both the clay matrix-dispersed microquartz and the quartz overgrowths observed under scanning electron microscopy are the products of clay transformation. For the reaction equation to hold, the process requires sufficient K^+. Whether the K^+ derives from the shale host rock itself or is transported from the surrounding strata is much debated. According to Fig. 2, Upper Longmaxi Formation in this study area has less potash feldspar and more illite than the Wufeng-Lower Longmaxi Formation. It is assumed that the dissolution of potash feldspar provides K^+ in the study area and generates relatively abundant microquartz in Upper Longmaxi Formation. The overall illite content in the study area is low and the transformation of 787.2 g of illite would theoretically generate only 197.7 g of silica (Boles and Franks, 1979). This indicates that the main source of silica for authigenic quartz in the study area is not related to clay mineral transformation.

The Al/(Fe + Al + Mn) ratio was used to determine the source of silica. A ratio of 0.01 indicates pure hydrothermal genesis while a ratio greater than 0.60 suggests pure biogenic genesis (Adachi et al., 1986; Yamamoto, 1987). The obtained Al/(Fe + Al + Mn) values for the samples in the study area range between 0.54 and 0.73 (Fig. 9). The Si/(Si + Al + Fe) ratio is also an important parameter for determining the source of silica, with higher values of biogenic ratios generally being greater than 0.9 (Liu et al., 2017). The obtained Si/(Si + Al + Fe) values for the

samples in the study area range from 0.61 to 0.92, with the shale parameter in the Wufeng-Lower Longmaxi Formation being closer to 0.9 (Fig. 9). It is observed that the authigenic quartz in the Wufeng-Lower Longmaxi Formation is dominated by biogenic quartz. The silica from both biogenic skeletal quartz and microquartz cements is derived from siliceous organisms. The main component of the siliceous planktonic carapace is opal-A, which dissolves and then precipitates or recrystallizes during burial to form quartz (Milliken et al., 2016).

The depositional environment of Wufeng-Lower Longmaxi Formation was the deep-water shelf and shale were deposited in an oxic water column environment (Lin et al., 2021). Marine water was abundant in siliceous organisms such as radiolarians and sponge spicules. The distance from terrestrial sources is moderate and the water environment is relatively quiet (Xu et al., 2004). The siliceous organisms could be preserved and buried in situ after death, thus the biogenic quartz content is high in Wufeng-Lower Longmaxi Formation. The depositional environment of Upper Longmaxi Formation was the shallow shelf. The sea level dropped during this period and the anoxic environment was destroyed, resulting in faster sedimentation rates and low siliceous organisms content. Xuefeng uplift became the main sediment source of the basin (Fig. 1). Due to more input of terrigenous clastic materials, the content of terrigenous quartz and clay minerals in Longmaxi is high in Upper Longmaxi Formation.

5.2 Percentage of quartz from different sources

The siliceous content derived from different sources can be approximately calculated based on the concentration of elements, which are terrigenous SiO_2, clay transformation SiO_2 and biogenic SiO_2. The quartz produced during the conversion from smectite to illite is primarily calculated based on Eq. (2) (van de Kamp, 2008):

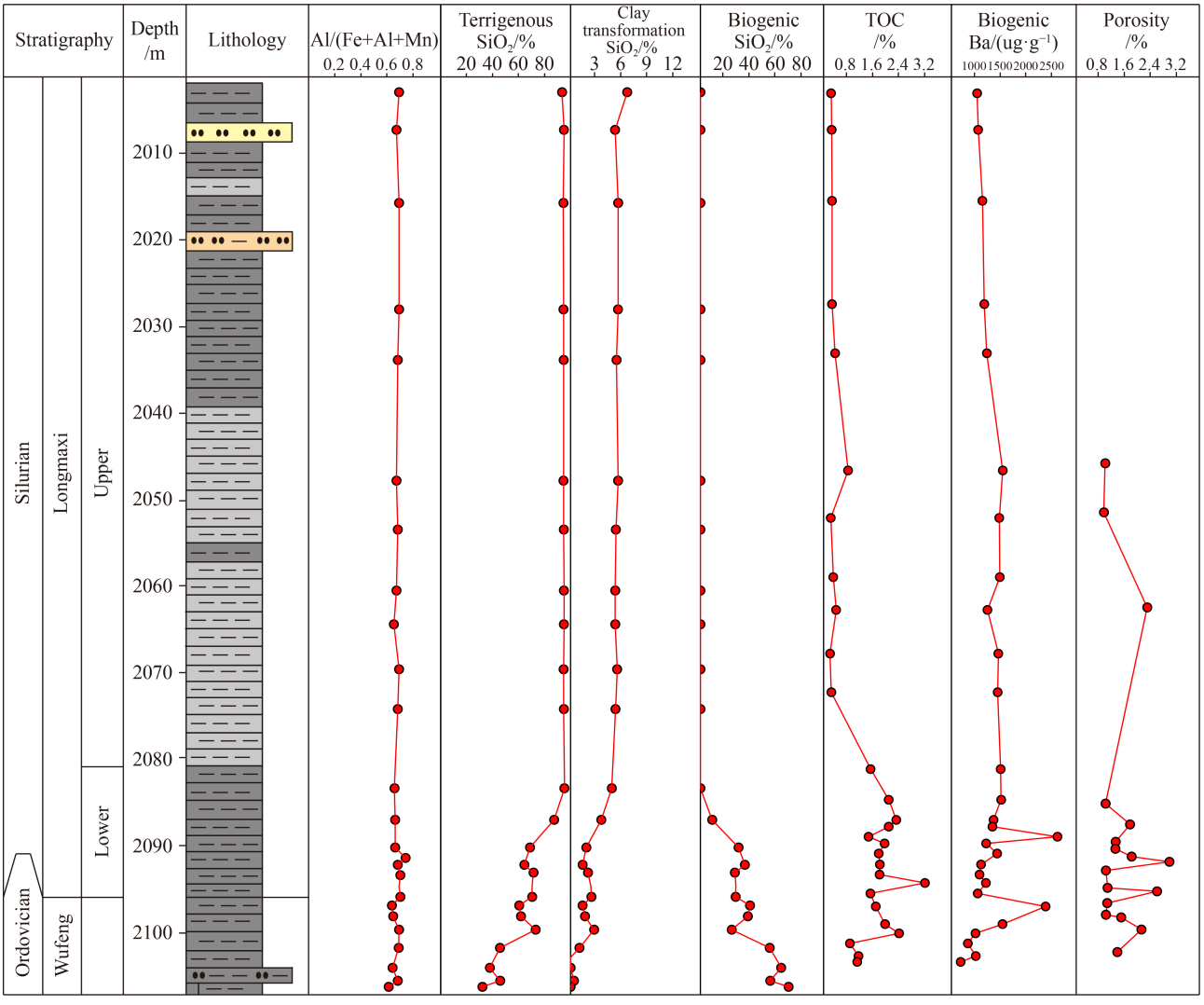

Fig. 9 Variation plot of relevant parameters versus depth for the shale samples of the Wufeng-Longmaxi Formation and the calculated values of different quartz sources.

$$1.308\,(Al_{3.15}Mg_{0.85})\,(Si_{8.00})\,O_{20}(OH)_4\,(Na_{0.85})\,2H_2O\ [\text{smectit}, 1101.1\text{g}] + (0.06Fe_2O_3 + 0.56K_2 + 0.02CaO) \rightarrow (Al_{4.12}Fe_{0.1}Mg_{0.56})\,(Si_{7.17})\,O_{20}(OH)_4\,(K_{1.47}Na_{0.01}Ca_{0.03})\ [\text{illite}, 787.2\text{g}]' + 3.29SiO_2[197.7\text{g}] + 0.56Na_2O + 0.55MgO + 3.23H_2O. \quad (2)$$

It is assumed that the total quantity of illite in the shale samples comes from the transformation of smectite. According to Eq. (1), a shale sample containing 787.2 g of illite produces 197.7 g of silica, therefore the amount of silica released by the clay mineral transformation process can be calculated from the illite content.

Excess Si content is defined as silica content above the normal detrital depositional environment and can be considered to represent biogenic silica. Excess Si is calculated by applying Eq. (3), where the $(Si/Al)_{background}$ value is 3.11 (Wedepohl, 1971; Tribovillard et al., 2006):

$$Si_{excess} = Si_{sample} - \left[(Si/Al)_{background} \times Al_{sample}\right]. \quad (3)$$

When the Si_{excess} value is obtained, the corresponding SiO_2 content can be calculated, i.e., the biogenic SiO_2 content. The terrigenous SiO_2 can be obtained by subtracting clay transformation SiO_2 and biogenic SiO_2 from the total SiO_2 content. The obtained results for calculating the content of quartz from different sources are shown in Fig. 9. The contents of different types of quartz in Upper Longmaxi Formation do not fluctuate with depth. The average content of terrigenous detrital quartz is 94%. The average content of clay transformation quartz is 6%, and there is basically no biogenic quartz. However, the content of different types of quartz in the Wufeng-Lower Longmaxi Formation varies significantly with depth. The content of terrigenous detrital quartz gradually decreases from 87% to 32%; clay transformation quartz gradually disappears from 5% downwards, while biogenic quartz increases from 9% to 68%.

5.3 Effect of quartz on organic matter accumulation

The TOC content gradually decreases from the bottom to the top, showing a direct correlation with changes in biogenic SiO_2 content (Fig. 9). The most essential condition for OM enrichment is for the water body to have high productivity, which can be represented by the biogenic Ba (Ba_{bio}) content. Numerous studies have shown that Ba_{bio} is related to marine productivity and is one of the main components for productivity calculation models (Francois et al., 1995). The Ba_{bio} content was estimated by subtracting the Ba from the detrital source and was calculated by using Eq. (4) (Yang et al., 2018):

$$Ba_{bio} = Ba_{tot} - Ti_{tot} \times (Ba/Ti)_{PAAS}, \quad (4)$$

where Ba_{tot} and Ti_{tot} represent the total Ba and Ti contents. $(Ba/Ti)_{PAAS}$ is the ratio of terrigenous Ba to Ti in the Post-Archean average Australian Shale (value taken as 0.11). As shown in Fig. 9, the high Ba content in the Wufeng-Lower Longmaxi Formation indicates that the marine waters were highly productive during this depositional phase. Marine waters were rich in siliceous organisms such as radiolarians and sponge spicules, which provided the necessary material for OM enrichment and production of biogenic SiO_2. Therefore, biogenic SiO_2 can be considered to a certain degree as a productivity parameter, showing a positive correlation with OM content.

5.4 Effect of quartz on pores

The porosity of the studied samples become higher with increased depth. The area with high porosity values is predominantly concentrated in the Wufeng-Lower Longmaxi Formation, and the variation of porosity is consistent with the biogenic quartz content (Fig. 9). Biogenic quartz formed mainly during early diagenesis. It created a crystalline structure that exhibits high hardness as well as high resistance to compression. The rigid framework formed by microquartz cements inhibited compaction and protected the original pore space (Guan et al., 2021). A significant amount of OM managed to be preserved in these pores (Fig. 10(a)).

The pores within solid bitumen are more abundant than those within kerogen, thus identifying solid bitumen from kerogen is important to evaluate the quality of the shale reservoir properly (Ko et al., 2016). If the migration of OM into the pores between authigenic minerals is observed, it can be inferred that the migration of OM occurs after cementation and that the OM is mainly solid bitumen (Bernard et al., 2012). Secondary nanopores develop mainly within the solid bitumen rather than within the deposited OM (Milliken et al., 2012). Solid bitumen is common in mature shale. As can be seen, the OM assigned to the quartz cements is solid bitumen (Fig. 10). When the sediments were in the oil window, the generated bitumen was discharged from the kerogen and transported into the interparticle pores and fractures of the quartz. The size and distribution range of the bitumen was controlled by the interparticle pores located between the microquartz cements. These OM particles eventually formed an OM network through the interparticle pores (Fig. 10(b)). As the maturity of the OM increased and a significant number of hydrocarbons were generated and expulsion began, OM pores were formed (Fig. 11). These OM pores were preserved by the rigid framework of quartz. and interconnected through interparticle pores and microfractures between quartz. As the primary pores are occupied by bitumen during hydrocarbon expulsion process, OM pores become the dominant factor in shale pore space (Zhao et al., 2017; Xie et al., 2021). Thus, biogenic quartz-rich shales possess high porosity, with OM pores contributing more to porosity than primary pores.

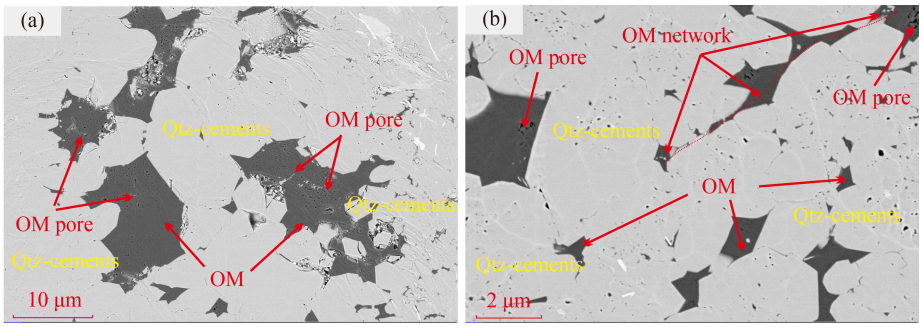

Fig. 10 SEM images of OM and quartz crystals: (a) a significant amount of OM filled the pores formed by the microquartz cements, and the OM pores created by the OM remained well preserved; (b) OM particles developed an OM network through interparticle pores.

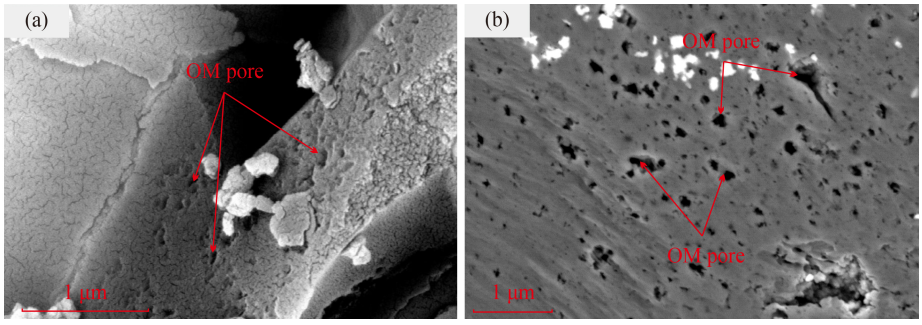

Fig. 11 SEM images of OM pores: (a) OM pores in unpolished samples; (b) OM pores in samples polished by the argon ion method.

During the experiment, it was determined that the local porosity varied extensively (Fig. 9), and two cases were considered: 1) the pores in the analyzed samples are primarily microporous. The limitations of the measurement method can lead to errors while measuring the porosity; 2) due to the barrier of clay minerals, the pores developed around the clay minerals only accommodate clay matrix-dispersed microquartz. This quartz is mainly flaky and fails to inhibit compaction (Xu et al., 2021). The quartz overgrowths occupied the interparticle pores between the terrigenous detrital quartz and other minerals (Fig. 3(c)). Metwally and Chesnokov (2012) demonstrated through simulation experiments that both types of quartz lead to a reduction in porosity. The low contents of clay-transformed quartz lead to the local reduction of porosity but do not affect the overall porosity change pattern.

5.5 Effect of quartz on shale brittleness

Guo et al. (2013) analyzed the brittleness of the Barnett shale in North America and concluded that the high Young's modulus and low Poisson's ratio indicate that the shale has higher brittleness characteristics. Based on these remarks, a brittleness index (BI) formula was proposed:

$$\mathrm{BI}=\frac{1}{2}\left(\frac{E-E_{\min}}{E_{\max}-E_{\min}}+\frac{\nu-\nu_{\max}}{\nu_{\min}-\nu_{\max}}\right)\times 100\%, \tag{5}$$

where E, $E_{\max}$, and $E_{\min}$ are Young's modulus, Young's modulus maximum, and Young's modulus minimum, respectively. ν, $\nu_{\max}$, and $\nu_{\min}$ are Poisson's ratio, Poisson's ratio maximum and Poisson's ratio minimum, respectively. In comparison with Upper Longmaxi Formation, Wufeng-Lower Longmaxi Formation has a higher Young's modulus and a lower Poisson's ratio, therefore it has better brittle properties. These brittle characteristics of the shales are directly related to the type, content and distribution of quartz. Terrigenous detrital quartz from the study area does not correlate well with the calculated BI values (R^2 = 0.0792) (Fig. 12(a)), while the BI values of biogenic quartz display a good positive correlation (R^2 = 0.6887) (Fig. 12(b)). This indicates that biogenic quartz has a noticeable effect on the brittleness of shale. Terrigenous detrital quartz tends to be distributed in the shale matrix, while authigenic quartz is mostly associated with minerals in the form of microquartz cements to apply a greater influence on the brittleness of the shale (Ye et al., 2020). Therefore, biogenic quartz-rich formations are more susceptible to the development of microfractures and facilitate the subsequent modification of fractures.

5.6 Formation mechanism of quartz

The formation of quartz from Wufeng-Longmaxi Formation can be divided into three stages (Fig. 13). 1) Deposition stage. The depositional environment during

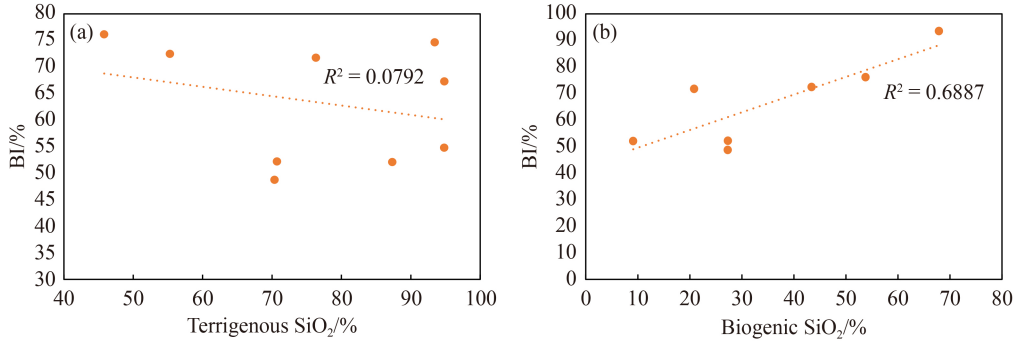

Fig. 12 Correlation plot between the brittleness index (BI) and (a) terrigenous SiO_2, (b) biogenic SiO_2.

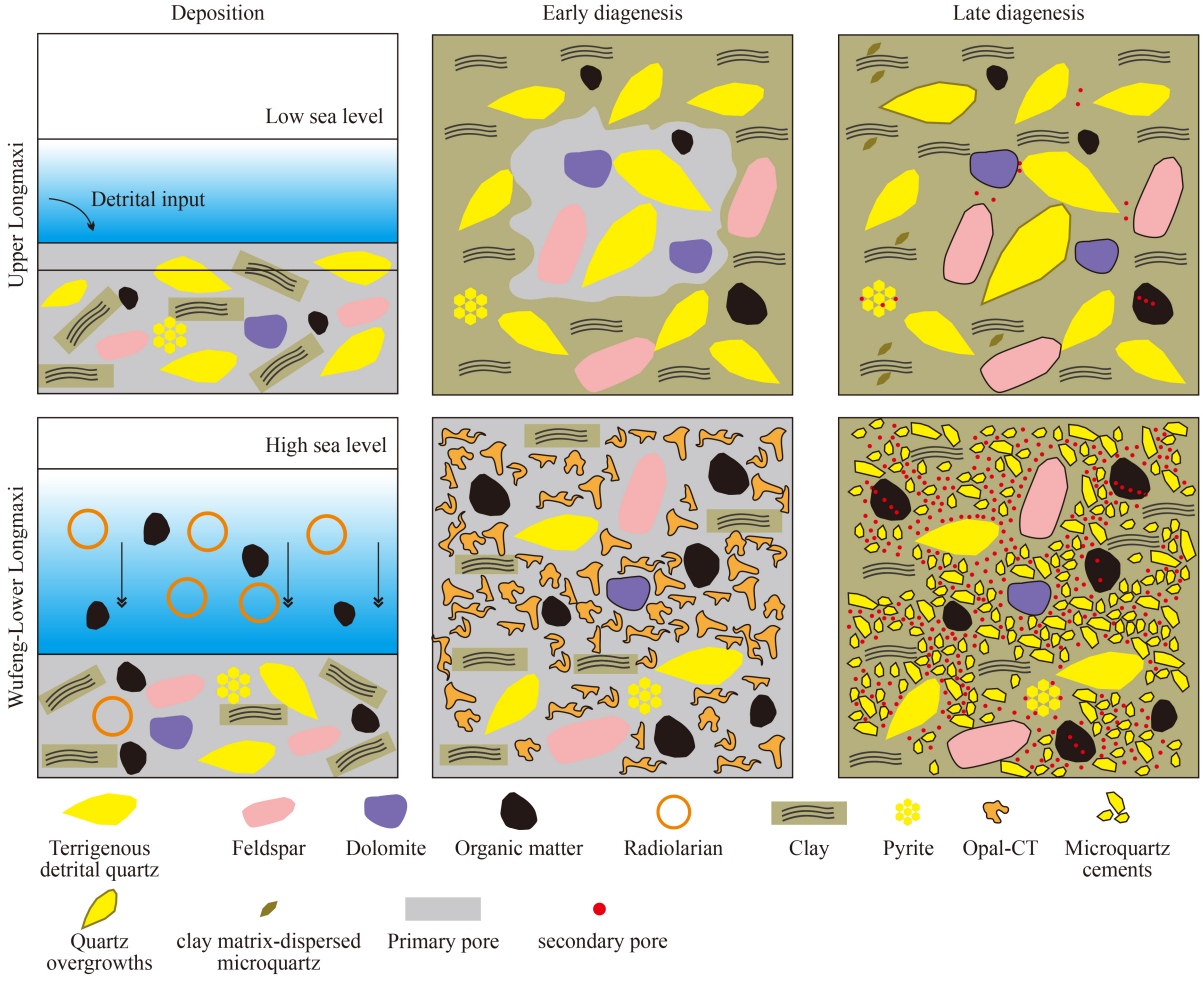

Fig. 13 Depositional and diagnesis model of the Wufeng-Longmaxi Formation shales.

the sedimentation of Wufeng-Lower Longmaxi Formation was characterized by high sea levels and anoxic marine conditions. The shale accumulated in the basin by suspension deposition as well as biological deposition, rich in OM and radiolarians. This was followed by marine regression, the sea levels dropped and the composition of Upper Longmaxi Formation shale was altered by the additional terrestrial input, which led to the deposition of large amounts of terrigenous detrital quartz (Xu et al., 2004). 2) Early diagenesis stage. The radiolarians encountered in shales of Wufeng-Lower Longmaxi Formation transformed into opal CT and eventually evolved into microquartz cements. This process inhibited compaction and served as a protection instrument for the primary pore spaces (Xi et al., 2019). In contrast, the primary pores of Upper Longmaxi shale were significantly reduced by compaction due to the lack of microquartz cements. 3) Late diagenesis stage. The OM pores and interparticle pores protected by microquartz cements in Wufeng-Lower Longmaxi Formation became

the space for shale gas enrichment. The clay transformation in Upper Longmaxi Formation shales led to the formation of quartz overgrowths around terrigenous detrital quartz or microquartz crystals in the clay matrix.

6 Conclusions

1) The quartz in the shales from the study area was classified into four major categories and five subcategories based on morphological features of SEM images, specifically terrigenous detrital quartz, quartz overgrowths, biogenic skeletal quartz and microquartz. Among these, the microquartz can be classified into clay matrix-dispersed microquartz and microquartz cements. The quartz in Upper Longmaxi Formation is predominantly of terrigenous origin but is also characterized by small amounts of quartz formed by clay transformation (quartz overgrowths and clay matrix-dispersed microquartz). Wufeng-Lower Longmaxi Formation is rich in authigenic quartz of biogenic origin, which is mostly present in the form of microquartz cements in the shales.

2) Biogenic quartz can be used to indicate a highly productive depositional environment, since the biogenic quartz-rich section is more abundant in OM. Biogenic quartz generally crystallizes during early diagenesis. The rigid framework formed by microquartz cements inhibits compaction and protects the pore space during diagenesis. The interparticle pores located between the quartz cements become the main space for OM accumulation and control the distribution of OM and OM pores.

3) The porosity of shale expands with the increase of bio-quartz content. However, terrigenous detrital quartz has little effect on porosity. Clay transformation quartz occupies the spaces of primary pores and leads to a decrease in porosity. By calculating the brittleness index, it has been determined that high biogenic quartz content is beneficial to the increase of shale brittleness. Biogenic quartz is more contributive to mechanical property of shale than the other types of quartz due to its special form of cementation.

Acknowledgments This study was financially supported by the National Science and Technology Major Project of China (No. 2017ZX05035). We thank all of the editors and reviewers for their helpful comments and suggestions.

References

Adachi M, Yamamoto K, Sugisaki R (1986). Hydrothermal chert and associated siliceous rocks from the northern pacific — their geological significance as indication of ocean ridge activity. Sediment Geol, 47(1–2): 125–148

Barghoorn E S, Tyler S A (1965). Microorganisms from the Gunflint Chert: these structurally preserved Precambrian fossils from Ontario are the most ancient organisms known. Science, 147(3658): 563–575

Bernard S, Horsfield B, Schulz H M, Wirth R, Schreiber A, Sherwood N (2012). Geochemical evolution of organic-rich shales with increasing maturity: a STXM and TEM study of the Posidonia Shale (Lower Toarcian, northern Germany). Mar Pet Geol, 31(1): 70–89

Boles J R, Franks S G (1979). Clay diagenesis in Wilcox sandstones of Southwest Texas: implications of smectite diagenesis on sandstone cementation. J Sediment Res, 49(1): 55–70

Chalmers G R, Bustin R M, Power I M (2012). Characterization of gas shale pore systems by porosimetry, pycnometry, surface area, and field emission scanning electron microscopy/transmission electron microscopy image analyses: examples from the Barnett, Woodford, Haynesville, Marcellus, and Doig units. AAPG Bull, 96(6): 1099–1119

Chung F H (1974). Quantitative interpretation of X-ray diffraction patterns of mixtures. I. Matrix-flushing method for quantitative multicomponent analysis. J App Crystallography, 7(6): 519–525

Curtis M E, Sondergeld C H, Ambrose R J, Rai C S (2012). Microstructural investigation of gas shales in two and three dimensions using nanometer-scale resolution imaging. AAPG Bull, 96(4): 665–677

Dong T, He S, Chen M F, Hou Y G, Guo X W, Wei C, Han Y J, Yang R (2019). Quartz types and origins in the paleozoic Wufeng-Longmaxi Formations, eastern Sichuan Basin, China: implications for porosity preservation in shale reservoirs. Mar Pet Geol, 106: 62–73

Francois R, Honjo S, Manganini S J, Ravizza G E (1995). Biogenic barium fluxes to the deep-sea – implications for paleoproductivity reconstruction. Global Biogeochem Cycles, 9(2): 289–303

Gambacorta G, Trincianti E, Torricelli S (2016). Anoxia controlled by relative sea-level changes: an example from the Mississippian Barnett Shale Formation. Palaeogeogr Palaeoclimatol Palaeoecol, 459: 306–320

Guan Q Z, Dong D Z, Zhang H L, Sun S S, Zhang S R, Guo W (2021). Types of biogenic quartz and its coupling storage mechanism in organic-rich shales: a case study of the Upper Ordovician Wufeng Formation to Lower Silurian Longmaxi Formation in the Sichuan Basin, SW China. Pet Explor Dev, 48(4): 813–823

Guo Z Q, Li X Y, Liu C, Feng X, Shen Y (2013). A shale rock physics model for analysis of brittleness index, mineralogy and porosity in the Barnett Shale. J Geophys Eng, 10(2): 025006

Ishii E, Sanada H, Iwatsuki T, Sugita Y, Kurikami H (2011). Mechanical strength of the transition zone at the boundary between opal-A and opal-CT zones in siliceous rocks. Eng Geol, 122(3–4): 215–221

Ko L T, Loucks R G, Zhang T W, Ruppel S C, Shao D Y (2016). Pore and pore network evolution of Upper Cretaceous Boquillas (Eagle Ford-equivalent) mudrocks: results from gold tube pyrolysis experiments. AAPG Bull, 100(11): 1693–1722

Li Y, Wang Z S, Gan Q, Niu X L, Xu W K (2019). Paleoenvironmental conditions and organic matter accumulation in Upper Paleozoic organic-rich rocks in the east margin of the Ordos Basin, China.

Fuel, 252: 172–187

Li Y, Yang J H, Pan Z J, Tong W S (2020). Nanoscale pore structure and mechanical property analysis of coal: an insight combining AFM and SEM images. Fuel, 260: 116352

Li Y, Chen J Q, Yang J H, Liu J S, Tong W S (2022). Determination of shale macroscale modulus based on microscale measurement: a case study concerning multiscale mechanical characteristics. Petro Sci, 19(3): 1262–1275

Lin D L, Tang S H, Xi Z D, Zhang B, Ye Y P (2021). Geochemical characteristics of Late Ordovician shales in the Upper Yangtze Platform, south China: implications for redox environmental evolution. Minerals (Basel), 11(7): 710

Liu J, Li Y, Zhang Y, Liu S, Cai Y (2017). Evidences of biogenic silica of Wufeng-Longmaxi Formation shale in Jiaoshiba area and its geological significance. J China U Petroleum (Nat Sci), 41(1): 34–41 (in Chinese)

Liu S G, Deng B, Li Z W, Sun W (2012). Architecture of basin-mountain systems and their influences on gas distribution: a case study from the Sichuan basin, South China. J Asian Earth Sci, 47: 204–215

Lynch F L (1997). Frio shale mineralogy and the stoichiometry of the smectite-to-illite reaction: the most important reaction in clastic sedimentary diagenesis. Clays Clay Miner, 45(5): 618–631

Metwally Y M, Chesnokov E M (2012). Clay mineral transformation as a major source for authigenic quartz in thermo-mature gas shale. Appl Clay Sci, 55: 138–150

Milliken K L, Ergene S M, Ozkan A (2016). Quartz types, authigenic and detrital, in the Upper Cretaceous Eagle Ford Formation, South Texas, USA. Sediment Geol, 339: 273–288

Milliken K L, Esch W L, Reed R M, Zhang T W (2012). Grain assemblages and strong diagenetic overprinting in siliceous mudrocks, Barnett Shale (Mississippian), Fort Worth Basin, Texas. AAPG Bull, 96(8): 1553–1578

Milliken K L, Olson T (2017). Silica diagenesis, porosity evolution, and mechanical behavior in siliceous mudstones, Mowry Shale (Cretaceous), Rocky Mountains, USA. J Sediment Res, 87(4): 366–387

Niu X, Yan D T, Zhuang X G, Liu Z X, Li B Q, Wei X S, Xu H W, Li D W (2018). Origin of quartz in the lower Cambrian Niutitang Formation in south Hubei Province, upper Yangtze platform. Mar Pet Geol, 96: 271–287

Peltonen C, Marcussen O, Bjorlykke K, Jahren J (2009). Clay mineral diagenesis and quartz cementation in mudstones: the effects of smectite to illite reaction on rock properties. Mar Pet Geol, 26(6): 887–898

Pommer M, Milliken K (2015). Pore types and pore-size distributions across thermal maturity, Eagle Ford Formation, southern Texas. AAPG Bull, 99(9): 1713–1744

Reynolds J H, Verhoogen J (1953). Natural variations in the isotopic constitution of silicon. Geochim Cosmochim Acta, 3(5): 224–234

Rowe H D, Loucks R G, Ruppel S C, Rimmer S M (2008). Mississippian Barnett Formation, Fort Worth Basin, Texas: bulk geochemical inferences and Mo-TOC constraints on the severity of hydrographic restriction. Chem Geol, 257(1–2): 16–25

Schieber J, Krinsley D, Riciputi L (2000). Diagenetic origin of quartz silt in mudstones and implications for silica cycling. Nature, 406(6799): 981–985

Shan C A, Zhang T, Wei Y, Zhang Z (2017). Shale gas reservoir characteristics of Ordovician-Silurian formations in the central Yangtze area, China. Front Earth Sci, 11(1): 184–201

Shimizu H, Masuda A (1977). Cerium in chert as an indication of marine environment of its formation. Nature, 266(5600): 346–348

Tatzel M, von Blanckenburg F, Oelze M, Bouchez J, Hippler D (2017). Late Neoproterozoic seawater oxygenation by siliceous sponges. Nat Commun, 8(1): 621

Thyberg B, Jahren J, Winje T, Bjorlykke K, Faleide J I, Marcussen O (2010). Quartz cementation in Late Cretaceous mudstones, northern North Sea: changes in rock properties due to dissolution of smectite and precipitation of micro-quartz crystals. Mar Pet Geol, 27(8): 1752–1764

Tribovillard N, Algeo T J, Lyons T, Riboulleau A (2006). Trace metals as paleoredox and paleoproductivity proxies: an update. Chem Geol, 232(1–2): 12–32

van de Kamp P C (2008). Smectite-illite-muscovite transformations, quartz dissolution, and silica release in shales. Clays Clay Miner, 56(1): 66–81

van den Boorn S H J M, van Bergen M J, Nijman W, Vroon P Z (2007). Dual role of seawater and hydrothermal fluids in Early Archean chert formation: evidence from silicon isotopes. Geology, 35(10): 939–942

Wedepohl K H (1971). Environmental influences on the chemical composition of shales and clays. Phys Chem Earth, 8: 307–333

Williams L A, Parks G A, Crerar D A (1985). Silica diagenesis, I. solubility controls. J Sediment Res, 55(3): 301–311

Wright J (2001). Making loess-sized quartz silt: data from laboratory simulations and implications for sediment transport pathways and the formation of ‘desert’ loess deposits associated with the Sahara. Quat Int, 76–77: 7–19

Xi Z D, Tang S H, Zhang S H, Yi Y X, Dang F, Ye Y P (2019). Characterization of quartz in the Wufeng Formation in northwest Hunan Province, south China and its implications for reservoir quality. J Petrol Sci Eng, 179: 979–996

Xi Z D, Tang S H, Zhang S H, Lash G G, Ye Y P (2022). Controls of marine shale gas accumulation in the eastern periphery of the Sichuan Basin, South China. Int J Coal Geol, 251: 103939

Xie W D, Wang M, Wang H, Ma R Y, Duan H Y (2021). Diagenesis of shale and its control on pore structure, a case study from typical marine, transitional and continental shales. Front Earth Sci, 15(2): 378–394

Xu C, Rong J Y, Yue L, Boucot A J (2004). Facies patterns and geography of the Yangtze region, South China, through the Ordovician and Silurian transition. Palaeogeogr Palaeoclimatol Palaeoecol, 204(3–4): 353–372

Xu H, Zhou W, Hu Q H, Yi T, Ke J, Zhao A K, Lei Z H, Yu Y (2021). Quartz types, silica sources and their implications for porosity evolution and rock mechanics in the Paleozoic Longmaxi Formation shale, Sichuan Basin. Mar Pet Geol, 128: 105036

Yamamoto K (1987). Geochemical characteristics and depositional environments of cherts and associated rocks in the Franciscan and Shimanto Terranes. Sediment Geol, 52(1–2): 65–108

Yang X R, Yan D T, Wei X S, Zhang L W, Zhang B, Xu H W, Gong Y, He J (2018). Different formation mechanism of quartz in siliceous and argillaceous shales: a case study of Longmaxi Formation in South China. Mar Pet Geol, 94: 80–94

Ye Y P, Tang S H, Xi Z D (2020). Brittleness evaluation in shale gas reservoirs and its influence on fracability. Energies, 13(2): 388

Zhao J H, Jin Z K, Jin Z J, Wen X, Geng Y K (2017). Origin of authigenic quartz in organic-rich shales of the Wufeng and Longmaxi Formations in the Sichuan Basin, south China: implications for pore evolution. J Nat Gas Sci Eng, 38: 21–38

Zhou L, Algeo T J, Shen J, Hu Z F, Gong H M, Xie S C, Huang J H, Gao S (2015). Changes in marine productivity and redox conditions during the Late Ordovician Hirnantian glaciation. Palaeogeogr Palaeoclimatol Palaeoecol, 420: 223–234

Zou C N, Yang Z, Sun S S, Zhao Q, Bai W H, Liu H L, Pan S Q, Wu S T, Yuan Y L (2020). “Exploring petroleum inside source kitchen”: shale oil and gas in Sichuan Basin. Sci China Earth Sci, 63(7): 934–953